



The effect of temperature on chromium vaporization and oxide scale growth on interconnect steels for Solid Oxide Fuel Cells



Hannes Falk-Windisch*, Jan Erik Svensson, Jan Froitzheim

The High Temperature Corrosion Centre, Chalmers University of Technology, 41296 Gothenburg, Sweden

HIGHLIGHTS

- Cr vaporization and oxide scale growth were studied at 650, 750 and 850 °C.
- Cr vaporization less affected by temperature than scale growth.
- Isothermal exposures did not show Arrhenius type Cr vaporization behavior.
- Paralineal mass gain behavior at 650 and 750 °C.

ARTICLE INFO

Article history:

Received 28 January 2015

Received in revised form

2 April 2015

Accepted 7 April 2015

Available online 8 April 2015

Keywords:

SOFC

Interconnect

Cr vaporization

Oxidation

Crofer

Sanergy

ABSTRACT

Chromium vaporization and oxide scale growth are probably the two most important degradation mechanisms associated with the interconnect in Solid Oxide Fuel Cells (SOFCs) when Cr₂O₃-forming alloys are used as the interconnect material. This study examines the influence of temperature on both mechanisms. Two commercially available steels; Crofer 22 H and Sanergy HT, were isothermally exposed at 650, 750 and 850 °C in an air-3% H₂O atmosphere with a high flow rate. Volatile chromium species were collected using the denuder technique. The microstructure of thermally grown oxide scales was characterized using Scanning Electron Microscopy (SEM), Energy Dispersive X-Ray Analysis (EDX) and X-Ray Diffraction (XRD). The findings of this study show that although Cr evaporation is reduced with lower temperature, its relative importance compared to oxide scale growth is greater.

© 2015 The Authors. Published by Elsevier B.V. This is an open access article under the CC BY-NC-ND license (<http://creativecommons.org/licenses/by-nc-nd/4.0/>).

1. Introduction

Solid Oxide Fuel Cell (SOFC) technology is seen as one of the future power sources with high potential for use due to its high overall efficiency, great fuel flexibility and clean emissions. To design a fuel cell system with the desired voltage, several cells must be connected in series to form a fuel cell stack. Each cell in the stack is separated and electrically connected with an interconnect. Some of the advantages of the SOFC, such as the ability to operate on a large variety of fuels without the need for an expensive catalyst, are associated with the high operating temperature which limits the choice of materials suitable for use as the interconnect.

The interconnect material must fulfil certain prerequisites. It must have a similar thermal expansion coefficient (TEC) compared

to the other ceramic parts in the cell, provide mechanical support to the stack, be gas tight, and have high electrical conductivity as well as low contact resistance with the electrodes. It must also be stable in both high p_{O2} (air on the cathode side) and in low p_{O2} (the fuel environment on the anode side) environments as well as inexpensive to manufacture [1]. The category of materials that seems to possess the combination of properties that best match these requirements for planar-type SOFC are Cr₂O₃-forming ferritic stainless steels. Although Cr₂O₃-forming alloys are generally considered to be fairly corrosion resistant, in the above environments, oxide scales that are several micrometre thick will grow at the interconnect surface [2] during the very long stack lifetime (>40 000 h), leading to high electrical contact resistance [3–5] and unacceptable stack degradation rates. Furthermore, a growing oxide layer is not the only mechanism that contributes to stack degradation when Cr₂O₃-forming alloys are applied as the interconnect material. The second degradation mechanism that shortens the service lifetime of the stack is cathode poisoning. Chromium (Cr) at the

* Corresponding author.

E-mail address: Hannes.windisch@chalmers.se (H. Falk-Windisch).

interconnect surface can be transported to the electrolyte–cathode–gas interface, called the triple phase boundary (TPB), either through diffusion or through vaporization [6–10]. The transported Cr may then either be reduced back to Cr(III) at the TPB, forming a deposit that blocks the electrochemical oxygen reduction process, or it may react with other stack components, contributing to rapid stack degradation [10–17]. Apart from cathode poisoning, Cr vaporization can be detrimental due to the depletion of Cr in the interconnect material. Once the Cr concentration of the material falls below a critical level fast growing Fe-rich oxide is formed, leading to breakaway corrosion. Volatile Cr species are formed at the interconnect surface when oxygen and water vapour react with the Cr-rich surface oxide. A number of volatile Cr species may form in a SOFC cathode environment, although several authors have shown that $\text{CrO}_2(\text{OH})_2$ is, by far, the most abundant volatile Cr species [18–21].

A number of commercially available steel grades have been developed specifically for SOFC applications. To reduce Cr vaporization, these steels have been alloyed with small amounts (0.3–0.5 wt.%) of Manganese (Mn), such as Crofer 22 APU and Crofer 22 H (ThyssenKrupp VDM), Sanergy HT (Sandvik Materials Technology) and ZMG 232 (Hitachi Metals). Sachitanand et al. and Stanislawski et al. [9,22] have shown that steels containing 0.3–0.5 wt.% Mn (including Crofer 22 APU, Crofer 22 H, Sanergy HT and ZMG 232) develop a well adherent $(\text{Cr,Mn})_3\text{O}_4$ spinel top layer above the Cr_2O_3 -layer at 800 and 850 °C, and that the rate of Cr vaporization for those alloys is 2–3 times lower than alloys that form pure Cr_2O_3 scales like Ducrolloy (Plansee), or a non-continuous $(\text{Mn,Cr})_3\text{O}_4$ top layer like E-brite (ATI Allegheny Ludlum). However, this reduction is not sufficient, and research focus has, therefore, shifted to mitigating Cr vaporization by applying various coating systems [7,23–31] or by developing new alternative Cr-free interconnect materials [32–34].

Nevertheless, the high operating temperature is by far the most dominant factor responsible for almost all degradation mechanisms within a stack. Intermediate Temperature SOFCs (IT-SOFCs) able to operate at temperatures as low as 500–700 °C [35] have, therefore, gained greater attention, and research focusing on enabling operation within this temperature range by developing new electrode and electrolyte materials has become an intensively studied field [36–41]. Longer lifetimes for SOFC systems and the possibility to utilize cheaper materials would be some of the potential benefits. It is commonly accepted that a lower temperature would attenuate the corrosion problems with the interconnect. Cr vaporization is also reduced at lower temperatures, however, according to several authors, a 100 °C decrease in temperature would lower Cr vaporization by only a factor of 2–3 [9,18,19,21]. Furthermore, Asteman et al. [42] have shown on a Cr_2O_3 -forming austenitic steel that Cr vaporization is substantial at temperatures as low as 600 °C. The majority of the research that includes both oxidation and Cr vaporization has been carried out at rather high temperatures (800 °C or higher) [7,24,26–31,43–45] to accelerate the degradation mechanisms mentioned above. However, since scale growth and Cr vaporization are two different degradation mechanisms, it is important to separate them and study the effect of temperature on both mechanisms separately.

For this reason, the present study examines both Cr vaporization and oxide scale growth in the temperature range of 650–850 °C.

2. Materials and methods

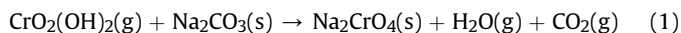
2.1. Materials

Two commercial interconnect materials, Sanergy HT (Sandvik Materials Technology AB) and Crofer 22 H (ThyssenKrupp VDM),

were selected for this study. Their compositions (weight %) are presented in Table 1. The samples were cut into $15 \times 15 \text{ mm}^2$ coupons and had a steel thickness of 0.2 mm. All samples were exposed in an as-received by the manufacturer state after being cleaned in acetone and ethanol using an ultrasonic bath.

2.2. Exposures

All exposures, containing three sample coupons each, were carried out in a horizontal tubular quartz reactor with an inner diameter of 46 mm. Both materials were exposed isothermally for 24, 168 and 500 h at 650, 750 and 850 °C in an air-3% H_2O environment with a flow rate of $6000 \text{ sml min}^{-1}$. 3% water vapour was achieved by bubbling the dried and cleaned air through a warm water bath connected to a condenser, which was set at 24.4 °C. In order to minimize natural convection, as well as to ensure a more uniform flow pattern, a porous silicon carbide flow restrictor was placed in front of the samples, standing parallel to the flow. A denuder tube made out of quartz was placed behind the samples to act as the reactor outlet. This tube had an inner diameter of 6 mm and the inside was coated with $\text{Na}_2\text{CO}_3(\text{s})$. Volatile Cr(VI) species formed at the sample surface were transported with the gas stream through the coated tube where sodium chromate was formed according to reaction [1].



The advantage of this technique is that the denuder tube can be replaced regularly and rinsed with water, without affecting the samples. The amount of vaporized Cr was then quantified using spectrophotometry (Evolution 60S, Thermo Scientific). A more detailed description of the denuder technique can be found elsewhere [28]. All exposures were repeated at least twice.

A second type of exposure was conducted to investigate the temperature dependency of Cr vaporization in a non-isothermal manner. The same setup and parameters as described above were used, but in contrast, the exposure was started at 850 °C and the temperature was lowered step-wise to 650 °C, as can be seen in Fig. 6.

2.3. Microstructural analysis

Gravimetric measurements were made using a six-decimal balance. The average net mass gain (change in mass before and after exposure) was calculated from three samples exposed simultaneously. The microstructure and chemical composition of the samples were analysed in an FEI Quanta 200 FEG Environmental Scanning Electron Microscope (ESEM) equipped with an Oxford Inca Energy Dispersive X-ray Spectroscopy (EDX) system. All microstructural analyses were performed under high vacuum mode utilizing a voltage of 15 kV. X-Ray Diffraction (XRD) measurements of the thermally grown oxide scales were carried out using a Siemens D5000 diffractometer with a grazing incidence setup. Cu-K α radiation was used and, depending on the oxide scale thickness, the angles of incidence were set to 1–5° to ensure penetration through the oxide to the substrate.

3. Results

3.1. Gravimetric analysis

Fig. 1 shows the net mass gain for the two steels, Sanergy HT and Crofer 22 H, exposed for 24, 168 and 500 h at 650, 750 and 850 °C. The exposures were carried out isothermally, i.e. each data point corresponds to a new set of samples. At 850 °C both steels exhibited

Table 1

Composition of the studied alloys in weight %, as specified by the manufacturer for the batches used.

| Material | Manufacturer | Fe | Cr | C | Mn | Si | Mo | W | Nb | RE |
|------------------------------|------------------------------|------|------|-------|------|------|------|-------|------|----|
| Sanergy HT Batch: 531816 | Sandvik Materials Technology | Bal. | 22.4 | 0.01 | 0.25 | 0.07 | 0.93 | <0.01 | 0.41 | Zr |
| Crofer 22 H Batch: 161061 | ThyssenKrupp VDM | Bal. | 22.9 | 0.007 | 0.4 | 0.2 | | 1.9 | 0.5 | La |

increasing net mass gains over time. The difference in net mass gain between the two steels increased over time, and, after 500 h, the observed net mass gains were 0.39 mg cm^{-2} (Sanergy HT) and 0.60 mg cm^{-2} (Crofer 22 H). At 750°C both steels showed lower net mass changes: Crofer 22 H exhibited a small but constantly increasing net mass gain over time (0.04 mg cm^{-2} after 500 h) whereas Sanergy HT only showed increased mass gain initially followed by a loss in mass over time (-0.04 mg cm^{-2} after 500 h). At 650°C , both steels showed an almost identical behaviour, indicating a minor increase in net mass within the first 24 h of exposure followed by a very small, almost linear, loss in mass with continued exposure time (approximately -0.02 mg cm^{-2} after 500 h for both steels).

3.2. Cr vaporization measurements

The measured amount of Cr vaporized as volatile Cr(VI) species for Sanergy HT and Crofer 22 H after 500 h of exposure is shown in Fig. 2. Both steels exhibited similar vaporization behaviour, although the amount of vaporized Cr was on average 20–30% lower after 500 h for Crofer 22 H irrespective of exposure temperature. Based on the data presented in Fig. 2 the rate of Cr vaporization as a function of time during isothermal exposure can be calculated and is illustrated in Figs. 3–5. The rates of Cr vaporization at 850°C indicate a reduction in the Cr vaporization rate as a function of time during the initial stage of exposure for both Sanergy HT and Crofer 22 H. The significant decrease in the Cr vaporization rate observed at 850°C for both steels took place within the first two weeks of exposure, followed by a steady-state rate of approximately $2.4 \times 10^{-4} \text{ mg cm}^{-2} \text{ h}^{-1}$. Moreover, Crofer 22 H showed a tendency for a more rapid decrease in vaporization rate than Sanergy HT. At 750°C both steels exhibited dissimilar vaporization rates after a certain amount of time during the isothermal exposure. Sanergy HT

displayed a minimal reduction in Cr vaporization rate in the initial stage of exposure, followed by a constant rate of approximately $2.1 \times 10^{-4} \text{ mg cm}^{-2} \text{ h}^{-1}$, which is almost the same rate as at 850°C after 500 h of exposure. Crofer 22 H, on the other hand, displayed a much more pronounced reduction at 750°C , which after 500 h of isothermal exposure resulted in a Cr vaporization rate of $\sim 9 \times 10^{-5} \text{ mg cm}^{-2} \text{ h}^{-1}$, which is half of the rate of Sanergy HT at 750°C after 500 h. At 650°C , the same trends were observed as at 750 and 850°C : A decrease in the Cr vaporization rate with time and a somewhat lower rate of Cr vaporization for Crofer 22 H than for Sanergy HT, although the difference between the two steels was not as pronounced as at the higher temperatures.

3.3. Cr vaporization on non-isothermal samples

It is reasonable to assume that there are compositional differences in the oxide scales formed at the different temperatures as well as variations over exposure time. In order to minimize such effects, a second set of exposures was carried out in which the samples were oxidized first at 850°C until a constant vaporization rate ($\sim 2.4 \times 10^{-4} \text{ mg cm}^{-2} \text{ h}^{-1}$) was observed. The temperature was then subsequently lowered to 750°C and 650°C , and Cr vaporization was measured. The rate of Cr vaporization for both steels can be seen in Fig. 6. In contrast to the isothermal exposures, both steels showed almost identical vaporization rates at all three temperatures after a certain initial exposure time at 850°C .

3.4. Microstructural investigation

Fig. 7 show the surface microstructure of Sanergy HT and Crofer 22 H at 650 , 750 and 850°C after 500 h of exposure, respectively. The surface oxide layer was continuous for both steels and no signs of spallation could be detected. Furthermore, oxide nodules could

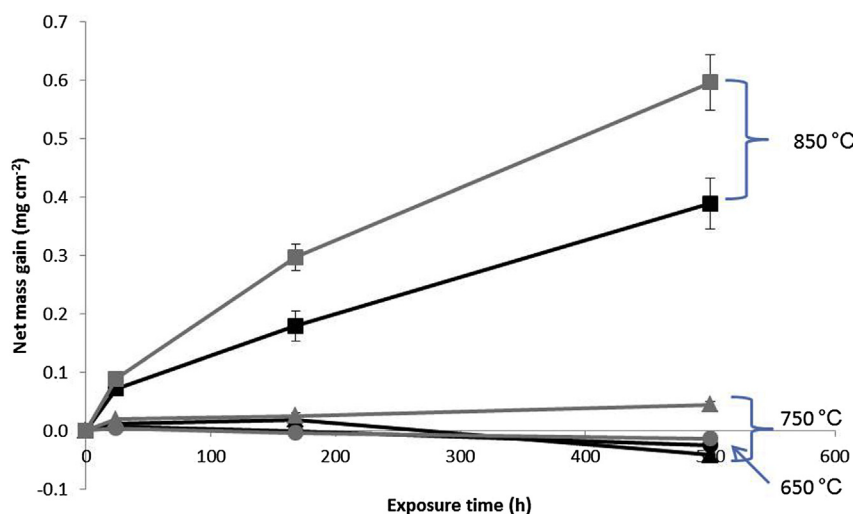


Fig. 1. Net weight change in Sanergy HT (black) and Crofer 22 H (grey) isothermally exposed for 24, 168 and 500 h at 650 (dots), 750 (triangles) and 850°C (squares) in air containing 3% H_2O .

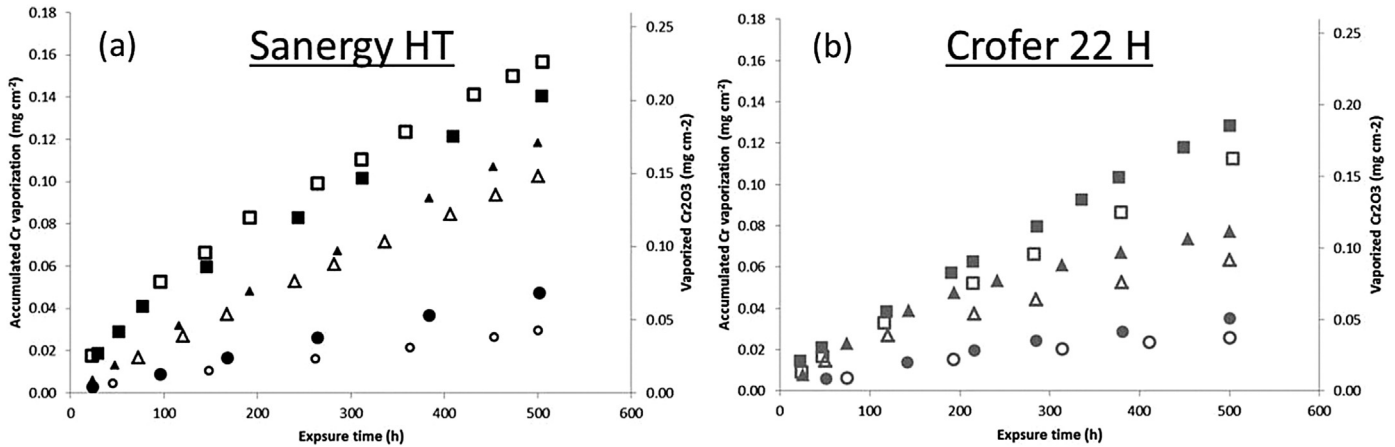


Fig. 2. Accumulated Cr vaporization as a function of time for (a) Sanergy HT and (b) Crofer 22 H at 650 (dots), 750 (triangles) and 850 °C (squares) in air containing 3% H₂O (6000 sml min⁻¹). Filled and empty symbols represent the two individual isothermal exposures.

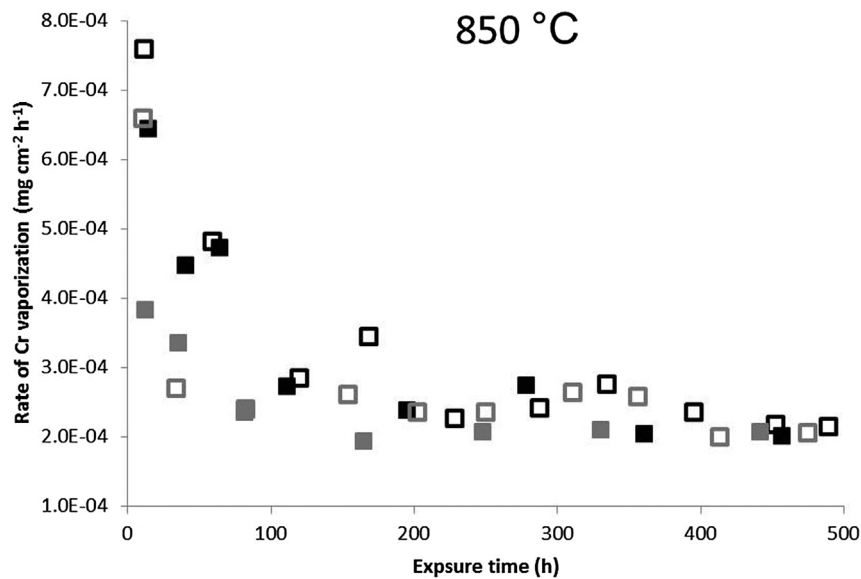


Fig. 3. Rate of Cr vaporization as a function of time for Sanergy HT (black) and Crofer 22 H (grey) at 850 °C in air containing 3% H₂O (6000 sml min⁻¹). Filled and empty symbols represent the two individual isothermal exposures.

be observed on both materials, especially on Sanergy HT at 750 °C. The elemental composition of these oxide nodules was similar to the main oxide scale. In addition to significantly fewer oxide nodules on the surface of Crofer 22 H at 750 °C, Fig. 8 shows that the grain size of the surface oxide was much larger for Crofer 22 H compared to Sanergy HT. Such a pronounced difference in the grain size of the surface oxide between the two steels was not observed at 650 and 850 °C. Cross sections including EDX elemental maps are shown in Fig. 9 for Sanergy HT and Crofer 22 H exposed for 500 h at 850 °C. Both steels formed a double-layered oxide and, in combination with the X-Ray Diffractograms shown in Fig. 10, it can be concluded that the inner layer was Cr₂O₃ and the outer layer was a (Cr,Mn)₃O₄ spinel-type oxide. In addition to the formation of a double-layered oxide, areas rich in both Cr and Mn, most probably spinel-type oxide, were observed close to the steel-oxide interface for Crofer 22 H. The oxide scales grown on the samples exposed at 650 and 750 °C were too thin for accurate SEM/EDX analysis and will therefore be investigated with TEM in a separate study. The XRD patterns in Fig. 10, however, showed that both Cr₂O₃ and

spinel-type oxide were formed at 650 and 750 °C after 500 h of exposure.

4. Discussion

4.1. Gross (corrected for Cr vaporization) weight change

Increased net mass can be directly correlated to the amount of oxygen that reacts with the steel, forming an oxide, i.e. scale growth. Changes in net mass values (Fig. 1) may, however, be misleading owing to factors such as vaporization or spallation of the oxide scale. This is obvious in the present study in which mass loss due to vaporization was significant or even dominated over mass gain at lower temperatures. Therefore, a reasonable comparison between the two materials can only be made by compensating for vaporization. By combining the net mass gain values in Fig. 1 with the Cr vaporization measurements in Fig. 2 it is possible to calculate gross mass gain compensated for the mass loss due to Cr vaporization. Fig. 11 shows such corrected gross mass gains in

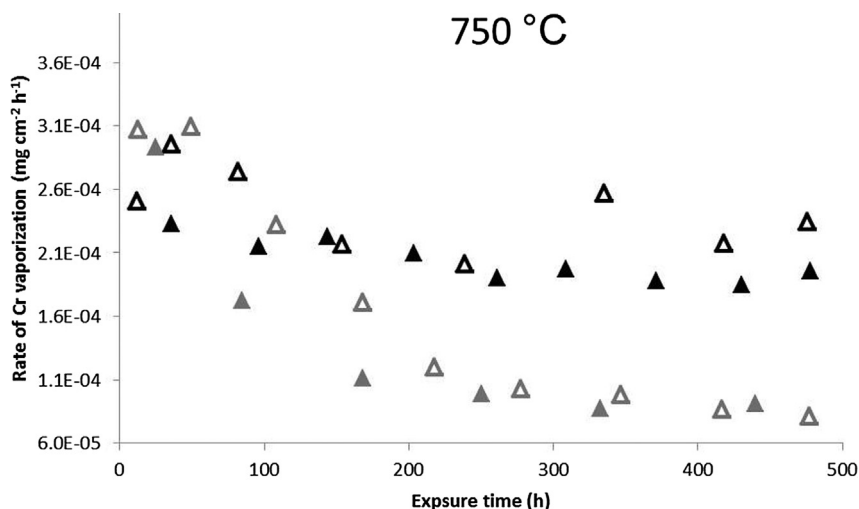


Fig. 4. Rate of Cr vaporization as a function of time for Sanergy HT (black) and Crofer 22 H (grey) at 750 °C in air containing 3% H₂O (6000 sml min⁻¹). Filled and empty symbols represent the two individual isothermal exposures.

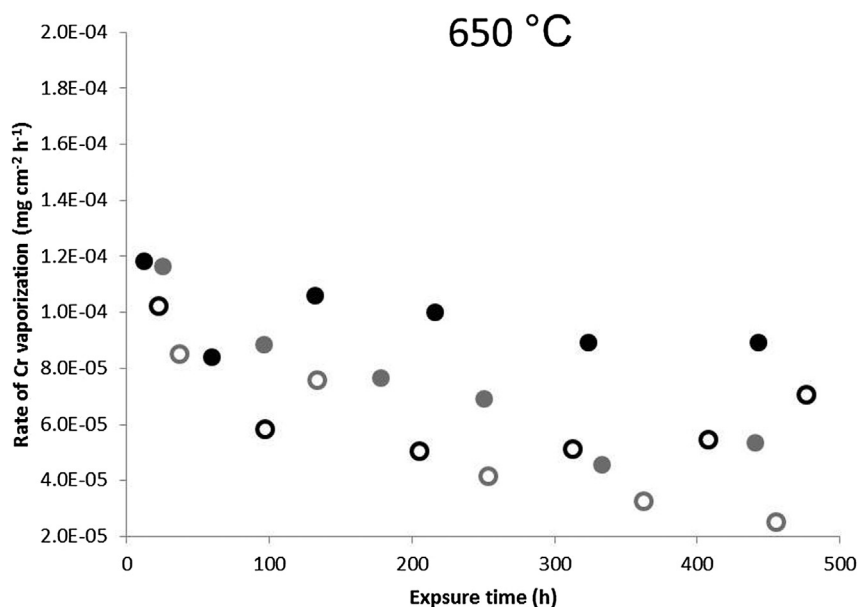


Fig. 5. Rate of Cr vaporization as a function of time for Sanergy HT (black) and Crofer 22 H (grey) at 650 °C in air containing 3% H₂O (6000 sml min⁻¹). Filled and empty symbols represent the two individual isothermal exposures.

which the amount of vaporized Cr has been calculated in relation to the mass of Cr₂O₃ and added to the initial net mass gain values. A more detailed description regarding this correction can be found in Sachitanand et al. [22].

4.2. Isothermal exposures at 850 °C

Both steels showed parabolic net mass gain behaviour at 850 °C (Fig. 1). The higher mass gain values for Crofer 22 H can partly be explained by the lower amount of vaporized Cr (Fig. 2). However, the corrected gross mass gain values (Fig. 11) suggest that higher net mass gain values for Crofer 22 H at 850 °C cannot be explained solely by the lower amount of vaporized Cr species. Instead, the higher net mass gain for Crofer 22 H is primarily due to the thicker oxide scale. The Cr₂O₃ layer was thicker on Crofer 22 H than on Sanergy HT and areas rich in Mn and Cr (probably spinel-type

oxide) were, in addition to the top oxide layer, observed in certain areas near the steel-oxide interface on Crofer 22 H (Fig. 9 (b)). Huczowski et al. have also observed such areas and have proposed that these Mn-rich oxides are formed as a result of “crack-healing” [46]. The thicker oxide scale is assumed to be correlated to the higher concentration of Mn in Crofer 22 H. Increased mass gain and decreased Cr vaporization at 850 °C with higher Mn content have been reported in an earlier study by Sachitanand et al. [22], which is in good agreement with the results obtained in this study. However, it should be pointed out that the Mn content in the steel is only one of several parameters that have an influence on the scale growth rate. Other alloying elements, microstructure and surface treatment also influence the scale growth rate. The reason for the decrease in Cr vaporization with Mn is generally connected to the formation of a continuous top layer of (Cr,Mn)₃O₄, which lowers the Cr activity at the surface of the material compared to Cr₂O₃. Both

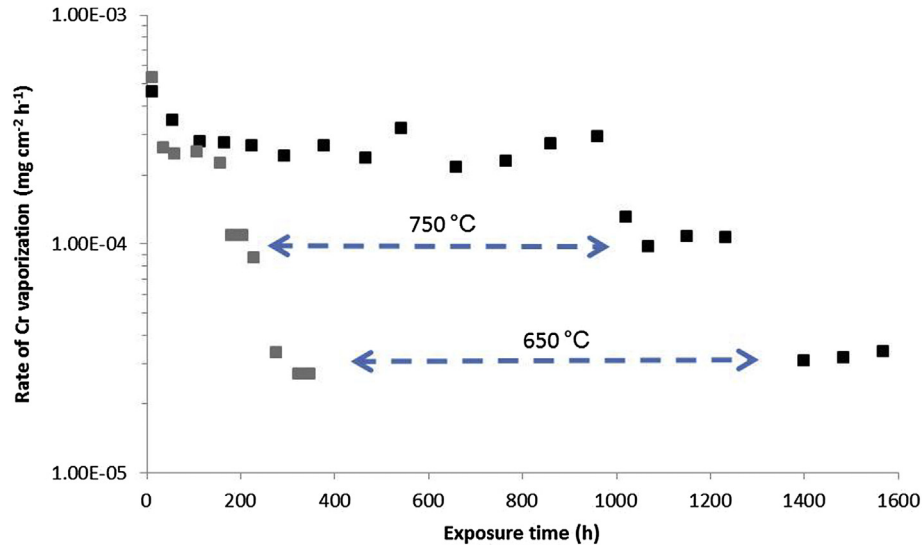


Fig. 6. Rate of Cr vaporization for Sanergy HT (black) and Crofer 22 H (grey) at different temperatures in air containing 3% H₂O (6000 sml min⁻¹). The samples were initially exposed at 850 °C until the rate of Cr vaporization was constant. In the very same exposure Cr vaporization was then measured at 750 and 650 °C.

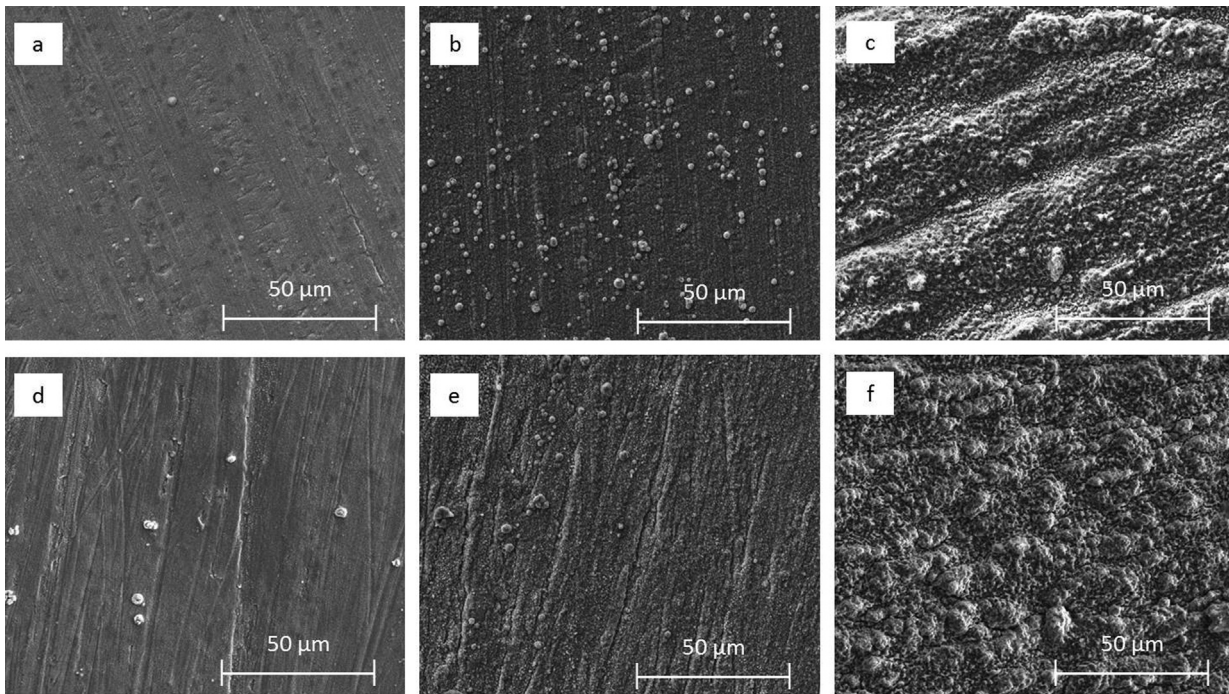


Fig. 7. SEM top view images of Sanergy HT exposed for 500 h at 650 (a) 750 (b) and 850 °C (c) and Crofer 22 H at 650 (d) 750 (e) and 850 °C (f) in air 3% H₂O (6000 sml min⁻¹).

steels in this study formed a continuous (Cr,Mn)₃O₄ surface layer after 500 h at 850 °C (Fig. 9). The thicknesses of these top layers are rather similar for the two steels, although the layer on Crofer 22 H seems to be slightly thicker than the one on Sanergy HT (1–2 μm compared to 1–1.5 μm).

As can be seen in Fig. 3, the rate of Cr vaporization at 850 °C levelled off to a value of approximately $2.4 \cdot 10^{-4}$ mg cm⁻² h⁻¹ for both steels after a certain amount of time of exposure, independent of Mn content. This observation fits well with the observation from Fig. 9 which show that the thickness of the (Cr,Mn)₃O₄ top layer after 500 h of exposure was rather similar for the two steels. It can, therefore, be assumed that the smaller total amount of vaporized Cr for Crofer 22 H is correlated to the faster decrease in the rate of

vaporization down to the mentioned steady-state rate of approximately $2.4 \cdot 10^{-4}$ mg cm⁻² h⁻¹. The formation and growth of an outer (Cr,Mn)₃O₄ spinel top layer is dependent on an outward flux of Mn, and, consequently, it is reasonable to assume that the faster decrease in the rate of vaporization is linked to the higher amount of Mn in Crofer 22 H. Although the formation of a continuous layer of (Cr,Mn)₃O₄ is the general explanation for a decrease in the rate of Cr vaporization, it should be pointed out that Froitzheim et al. [27] have observed an Mn and Cr-rich outer oxide layer on Sanergy HT after only one hour of exposure at 850 °C, suggesting that the surface was already covered by a very thin (Cr,Mn)₃O₄ top layer. Since Fig. 3 clearly shows that it takes several days, and not hours, to reach the steady-state rate some other mechanism is suspected

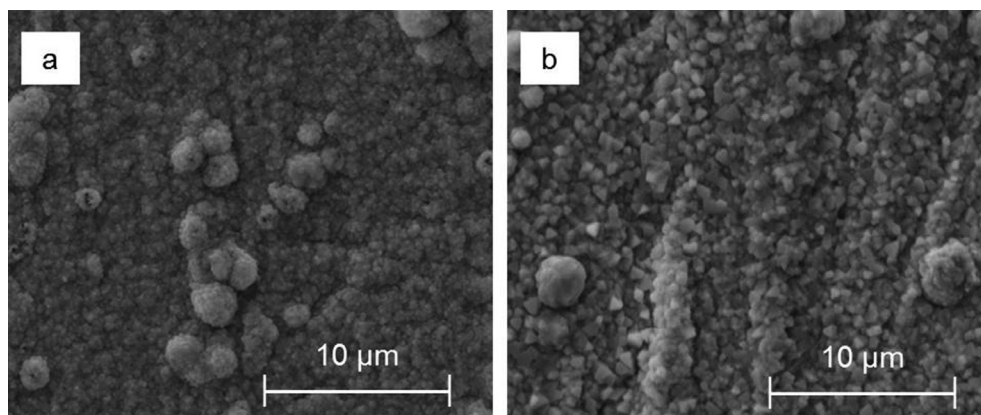


Fig. 8. SEM top view images of Sanergy HT (a) and Crofer 22 H (b) exposed for 500 h at 750 °C in air 3% H₂O (6000 sml min⁻¹).

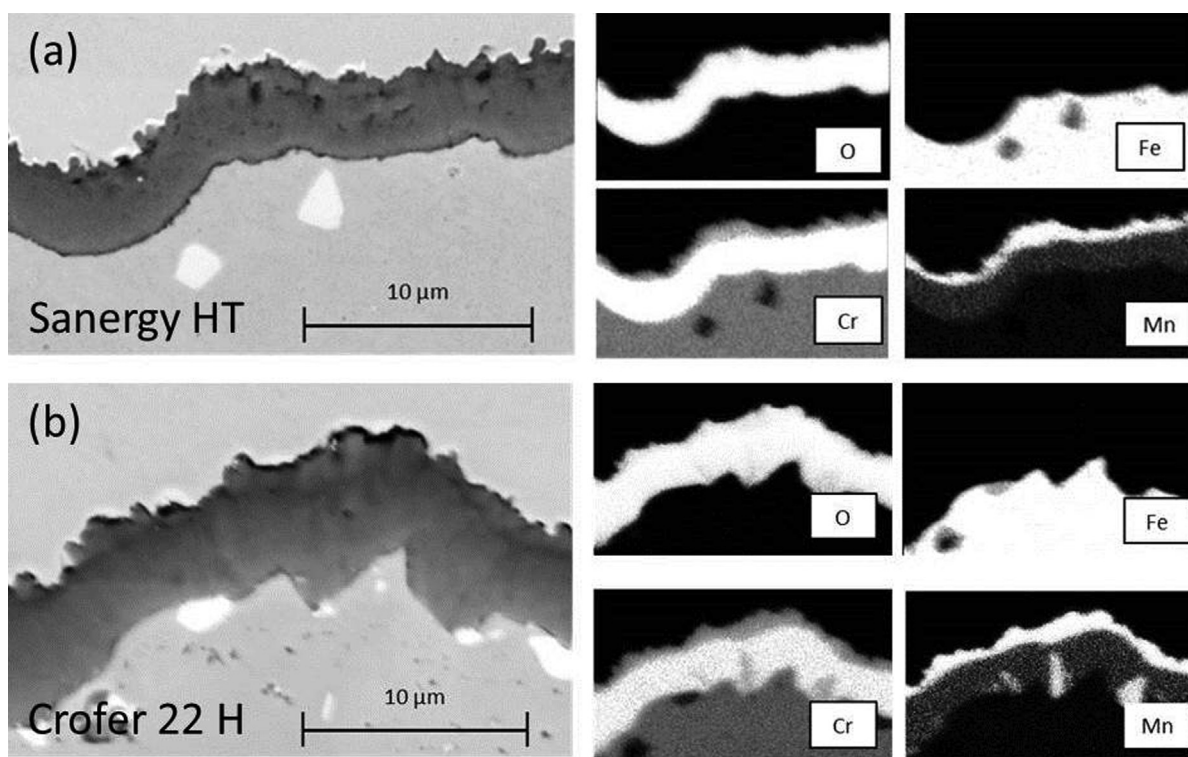
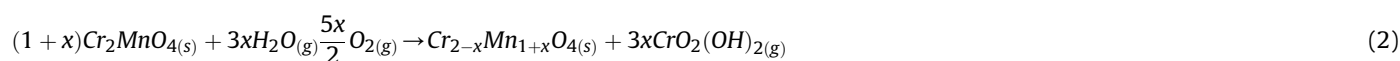


Fig. 9. SEM cross section and EDX elemental maps of (a) Sanergy HT and (b) Crofer 22 H exposed for 500 h at 850 °C in air 3% H₂O (6000 sml min⁻¹).

to govern the reduction in the rate of Cr vaporization than just the formation of a (Cr,Mn)₃O₄ top layer. Assuming that the formation of volatile Cr (VI) species only takes place at the surface (atoms in contact with the gas phase) one would not expect a direct effect on the oxide thickness as long as the chemical composition is the same throughout the oxide layer. However, since an oxide scale grows in non-equilibrium conditions one could assume that a chemical gradient may be present within the scale. Due to the large miscibility in (Cr,Mn)₃O₄ at 850 °C, the Cr:Mn ratio could vary from 2:1 (Cr₂MnO₄) to below 1:2 (~Mn₂CrO₄) [47]. Since Fig. 3 clearly

indicates that the rate of vaporization decreases with time over a period of several days until the steady-state rate is reached, it can be assumed that the Cr activity in the (Cr,Mn)₃O₄ top oxide layer also decreases until a certain composition (which may be similar for both steels at the steady-state rate) has been attained. In the initial hour of exposure, when this top layer is extremely thin, the Cr activity may be very high. However, when the layer becomes thicker a concentration gradient may arise due to rapid Mn outward diffusion as well as the loss of Cr due to vaporization according to [2].



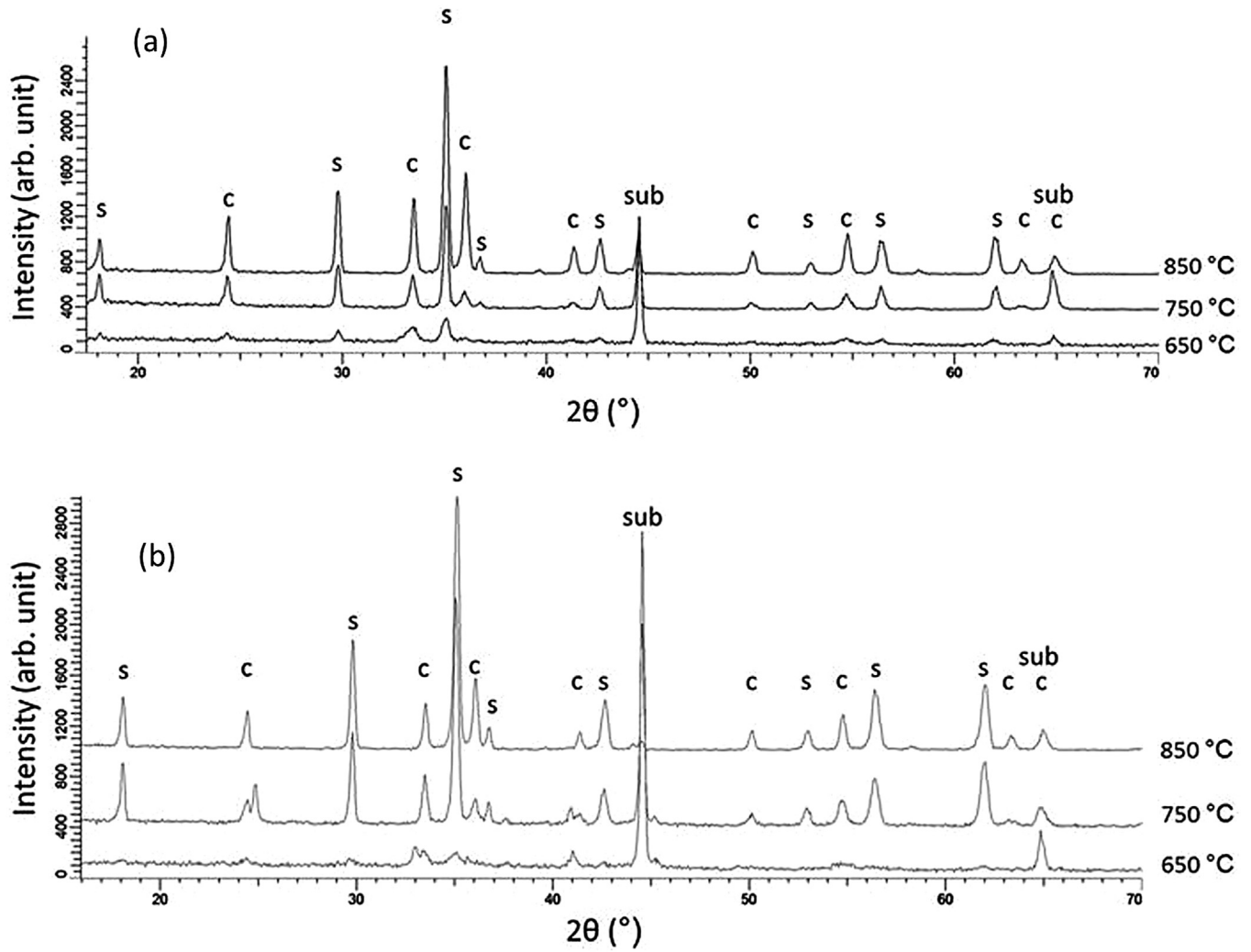


Fig. 10. XRD diffractograms for (a) Sanergy HT and (b) Crofer 22 H exposed for 500 h at 650, 750 and 850 °C in air 3% H_2O ($6000 \text{ sml min}^{-1}$). The symbols indicate: spinel type oxide M_3O_4 (s), chromia, Cr_2O_3 (c) and the ferritic stainless steel (sub).

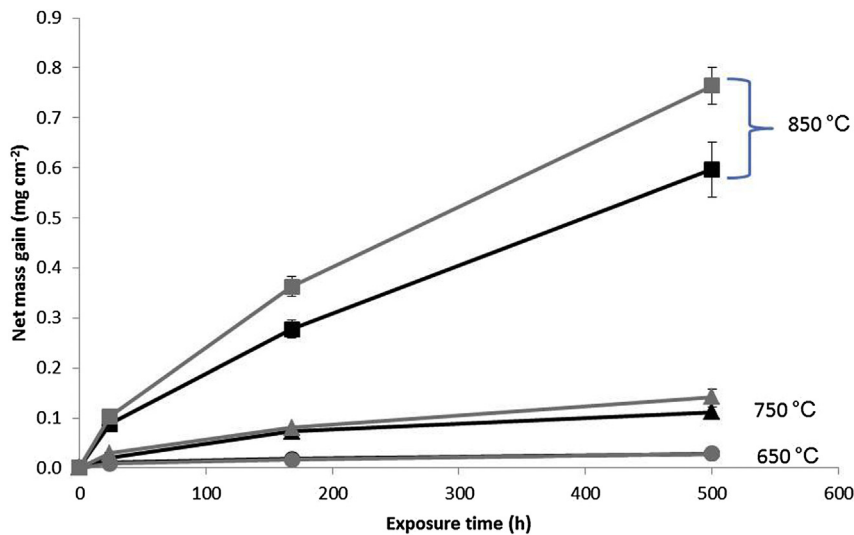


Fig. 11. Gross (corrected for Cr vaporization) weight change in Sanergy HT (black) and Crofer 22 H (grey) isothermally exposed for 24, 168 and 500 h at 650 (dots), 750 (triangles) and 850 °C (squares).

This proposal is in good agreement with the observation by Canovic et al. [48] of Sanergy HT oxidized for 168 h at 850 °C. Canovic et al. have observed a concentration gradient through the (Cr,Mn)₃O₄ top layer with a Cr:Mn ratio of approximately 2:1 at the chromia-spinel interface with a slight increase in Mn concentration towards the surface of the oxide scale.

4.3. Isothermal exposures at 750 °C

When the temperature was decreased to 750 °C much smaller changes in weight were observed. At this temperature the enhanced relative effect of Cr vaporization became obvious. Crofer 22 H showed a very small net mass gain whereas Sanergy HT actually showed a negative net mass gain after 500 h of exposure (Fig. 1). The observed negative net mass gain for Sanergy HT after 500 h at 750 °C is not due to spallation of the oxide scale, since no sign of spallation on the surface could be detected and since the scales grown at lower temperatures were much thinner than the corresponding non-spalling scales grown at 850 °C. Tedmon has described the net mass change behaviour when an oxide scale grows parabolically but is simultaneously vaporized [49]. If the rate of vaporization is high enough, an initial net mass gain will be observed followed by a linear mass loss (paralinear oxidation). In the initial phase of oxidation, solid state diffusion is rapid due to the thin oxide scale, which gives rise to parabolic net mass gain behaviour. However, after a certain limiting oxide scale thickness, the rate of oxide scale growth will be equal to the rate of vaporization. At this point, the thickness of the oxide scale will remain constant and a linear mass loss will be observed due to the loss of Cr in the alloy. This was not observed at 850 °C since the rate of scale growth was much faster than the rate of vaporization. At 750 °C, however, solid state diffusion through the oxide scale was much slower, whereas the rate of Cr vaporization was much less affected by the decrease in temperature. It is, therefore, proposed that the negative net mass gains observed for Sanergy HT under the present conditions is attributed to the enhanced influence of Cr vaporization on the net mass change at lower temperatures. This assumption is strongly supported by the illustration in Fig. 11 which shows that both steels actually behaved almost identically when the net mass gain had been compensated for vaporization (gross mass gain). It is, therefore, important to point out that without correcting the net mass gain for Cr vaporization one may be misled into believing that materials that vaporize more Cr, such as Sanergy HT, show better corrosion properties due to the lower recorded net mass gain.

The total amount of vaporized Cr at 750 °C was lower for the Mn-richer steel Crofer 22 H than for Sanergy HT (Fig. 2). The rate of Cr vaporization was reduced with time (Fig. 4), as was the case at 850 °C. The amount of time it took to reduce the rate of Cr vaporization was, however, longer than at 850 °C. Due to the lower temperature, diffusion was significantly slower, which probably explains why the decrease in the rate of vaporization took a longer amount of time at 750 °C than at 850 °C for Crofer 22 H. Sanergy HT, on the other hand, only showed a minimal reduction initially, followed by an almost constant rate of approximately $2.1 \cdot 10^{-4}$ mg cm⁻² h⁻¹. According to the XRD data (Fig. 10) both steels formed chromia and spinel phases at 750 °C. Due to the very thin nature of those oxide scales (<500 nm) SEM/EDX analysis could not reveal sufficient information about their chemical composition and microstructure. However, since both the Mn content in the steel and the net mass gain after 500 h was higher for Crofer 22 H, it is believed that the top spinel layer was thicker on Crofer 22 H than on Sanergy HT. Furthermore, the top view SEM images (Fig. 8) indicate that the surface on Crofer 22 H was covered by larger crystallites, suggesting the formation of a thicker and

more pronounced spinel top layer. If the spinel top layer was thicker for Crofer 22 H, the same argument as for the samples exposed at 850 °C could be made; that a thicker oxide layer leads to a chemical gradient with a decrease in the concentration of Cr towards the oxide scale surface.

4.4. Isothermal exposures at 650 °C

When the temperature was decreased to 650 °C very small net mass gains were initially observed, followed by negative net mass gains for both Sanergy HT and Crofer 22 H after 500 h of exposure (Fig. 1). This type of oxidation kinetics, paralinear oxidation was discussed in Section 4.3. In contrast to 750 °C, both steels showed linear mass loss after only 24 h of exposure at this temperature. The amount of vaporized Cr species after 500 h of exposure was even lower at 650 °C than at 750 and 850 °C. It seems that the same trend, i.e. that Crofer 22 H vaporize less than Sanergy HT, was valid for 650 °C as well, but the small difference in Cr vaporization was within the variation of each individual exposure. By compensating for Cr vaporization it became evident that both steels showed small positive gross mass gains, as was expected (Fig. 11). The formation of both chromia and spinel phases at 650 °C was confirmed with XRD (Fig. 10) as at 750 and 850 °C. Further analysis of the oxide scales was not carried out in this study since these were extremely thin (~100 nm).

4.5. Effect of temperature on oxide scale growth and Cr vaporization

To study the influence of temperature on oxide scale growth, as well as to compare scale growth to Cr vaporization, the activation energy for both reactions was calculated utilizing Equation (3).

$$\ln(k) = \frac{-E_a}{RT} + \ln(A) \quad (3)$$

where k is the rate constant of a chemical reaction (oxide scale growth respective Cr vaporization), E_a is the activation energy, R is the universal gas constant, T is the absolute temperature and A is the pre-exponential factor.

4.5.1. Activation energy calculations for oxide scale growth

To calculate the activation energy for oxide scale growth, parabolic rate constants were calculated from the gross mass gain data (Fig. 11). The relationship between mass gain and oxidation kinetics can be described by the parabolic rate law.

$$\left(\frac{\Delta m}{A}\right)^2 = k_p t + C \quad (4)$$

where, Δm is the mass gain, A is the sample surface area, t is the exposure time, C is the integration constant and k_p is the parabolic rate constant. Parabolic rate constants were calculated by plotting squared gross mass gain (corrected mass gain from Fig. 11) as a function of exposure time. Both steels showed parabolic behaviour indicating that scale growth is controlled by solid state diffusion.

Table 2
Parabolic rate constants (k_p) for Sanergy HT and Crofer 22 H at 650, 750 and 850 °C in air containing 3% H₂O (6000 sml min⁻¹).

| | | 650 °C | 750 °C | 850 °C |
|-------------|--|----------------------|----------------------|----------------------|
| Sanergy HT | mg ² cm ⁻⁴ h ⁻¹ | $1.6 \cdot 10^{-6}$ | $2.5 \cdot 10^{-5}$ | $7.2 \cdot 10^{-4}$ |
| | g ² cm ⁻⁴ s ⁻¹ | $4.5 \cdot 10^{-16}$ | $7.0 \cdot 10^{-15}$ | $2.0 \cdot 10^{-13}$ |
| Crofer 22 H | mg ² cm ⁻⁴ h ⁻¹ | $1.6 \cdot 10^{-6}$ | $4.1 \cdot 10^{-5}$ | $1.2 \cdot 10^{-3}$ |
| | g ² cm ⁻⁴ s ⁻¹ | $4.5 \cdot 10^{-16}$ | $1.1 \cdot 10^{-14}$ | $3.3 \cdot 10^{-13}$ |

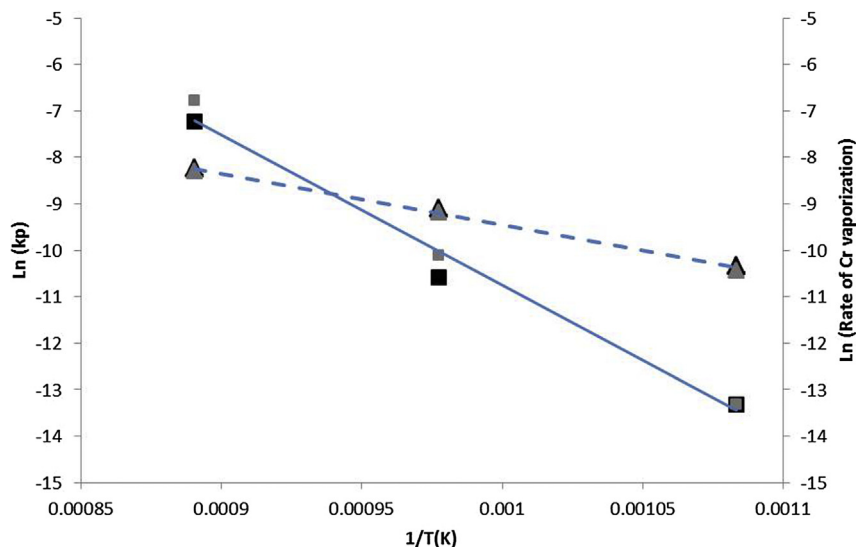


Fig. 12. Arrhenius plot showing the influence of temperature on both scale growth (squares) utilizing the parabolic rate constants from Table 2 and the rate of Cr vaporization from Fig. 6 (triangles) for Sanergy HT (black) and Crofer 22 H (grey) in air containing 3% H₂O (6000 sml min⁻¹).

The calculated rate constants for the two steels at 650, 750 and 850 °C can be seen in Table 2. These values are within the typical order of Cr₂O₃-forms [50–52]. The obtained activation energies for scale growth were 261 and 283 kJ mol⁻¹ for Sanergy HT and Crofer 22 H, respectively (see Fig. 12), which agrees well with other published activation energy values for the oxidation of Fe–Cr alloys in air [50,53–56]. These values were compared to the 255 kJ mol⁻¹ reported by Hagel and Seybolt [57] for cation diffusion in Cr₂O₃, suggesting that the oxide scale predominantly grows by means of the outward diffusion of Cr ions. However, it is more likely that this value is a combination of several mechanisms and is specific for the alloys and exposure conditions.

4.5.2. Activation energy calculations for Cr vaporization

It was not possible to calculate the activation energies for Cr vaporization on isothermally exposed samples since Sanergy HT, specifically, did not show Arrhenius-type behaviour. This is assumed to be due to differences in chemical composition or/and morphology at various temperatures. Fig. 12 shows the Arrhenius plot for Cr vaporization on the non-isothermally exposed samples (Fig. 6). The calculated activation energies were 91 and 92 kJ mol⁻¹ for Sanergy HT and Crofer 22 H, respectively. These values are in good agreement with the 83 kJ mol⁻¹ for Cr vaporization on a Cr₂O₃ surface theoretically calculated by Panas et al. [58].

Fig. 12 clearly shows that temperature had a greater effect on oxide scale growth than Cr vaporization (activation energy being approximately 270 kJ mol⁻¹ for oxide scale growth and 90 kJ mol⁻¹ for Cr vaporization). By reducing the temperature 100 °C, the amount of vaporized Cr only decreased by a factor 2–3, whereas the gross mass gain decreased by a factor of five. Furthermore, the observed net mass losses at lower temperatures clearly point out the increased relevancy of Cr vaporization at lower temperatures. It is, therefore, important to include the vaporization factor when lifetime estimations are carried out. Furthermore, to ensure stable long-term performance in a SOFC stack, high quality coatings that inhibit Cr vaporization are necessary, even if the operating temperature is decreased to temperatures as low as 650 °C.

5. Conclusions

The results show that both steels, Sanergy HT and Crofer 22 H,

formed oxide scales consisting of Cr₂O₃ and (Cr,Mn)₃O₄ at all three temperatures measured. Both steels showed rather similar oxidation and vaporization behaviour.

Although Cr evaporation is reduced with lower temperature, its relative importance compared to oxide scale growth becomes greater. A 100 °C decrease in temperature reduced the gross mass gain by a factor of 5 whereas Cr vaporization was only reduced by a factor of 2–3. This resulted in a change in oxidation kinetics from parabolic to parabolic oxidation kinetics when the temperature was reduced from 850 °C to 750 and 650 °C.

These findings, consequently, point out the importance of accounting for Cr vaporization when lifetime predictions are carried out, especially at the lower operating temperatures.

Furthermore, increased temperature as an method for accelerated life-time testing may be misleading due to differences in chemical composition or/and morphology at various temperatures.

Acknowledgements

The financial support received from The Swedish Research Council and the Swedish Energy Agency (Grant Agreement No 34140-1), The Swedish High Temperature Corrosion Centre as well as the Nordic NaCoSOFC project is gratefully acknowledged. Furthermore, the funding received from the European Union's Seventh Framework Programme (FP7/2007-2013) for the Fuel Cells and Hydrogen Joint Technology Initiative under grant agreement n° [278257] is gratefully acknowledged.

References

- [1] J.W. Fergus, *Mat. Sci. Eng. a-Struct.* 397 (2005) 271–283.
- [2] N.H. Menzler, P. Batfalsky, S.M. Gross, V. Shemet, F. Tietz, *Ecs Trans.* 35 (2011) 195–206.
- [3] L. Barelli, E. Barluzzi, G. Bidini, *Int. J. Hydrogen Energy* 38 (2013) 5060–5074.
- [4] J.I. Gazzarri, O. Kesler, *J. Power Sources* 176 (2008) 138–154.
- [5] W.Z. Zhu, S.C. Deevi, *Mater. Res. Bull.* 38 (2003) 957–972.
- [6] E. Konyshcheva, H. Penkalla, E. Wessel, J. Mertens, U. Seeling, L. Singheiser, K. Hilpert, *J. Electrochem. Soc.* 153 (2006) A765–A773.
- [7] H. Kurokawa, C.P. Jacobson, L.C. DeJonghe, S.J. Visco, *Solid State Ionics* 178 (2007) 287–296.
- [8] G.Y. Lau, M.C. Tucker, C.P. Jacobson, S.J. Visco, S.H. Gleixner, L.C. DeJonghe, *J. Power Sources* 195 (2010) 7540–7547.
- [9] M. Stanislawski, E. Wessel, K. Hilpert, T. Markus, L. Singheiser, *J. Electrochem. Soc.* 154 (2007) A295–A306.

- [10] M.C. Tucker, H. Kurokawa, C.P. Jacobson, L.C. De Jonghe, S.J. Visco, J. Power Sources 160 (2006) 130–138.
- [11] S.P.S. Badwal, R. Deller, K. Foger, Y. Ramprakash, J.P. Zhang, Solid State Ionics 99 (1997) 297–310.
- [12] X.B. Chen, L. Zhang, E.J. Liu, S.P. Jiang, Int. J. Hydrogen Energy 36 (2011) 805–821.
- [13] J.W. Fergus, Int. J. Hydrogen Energy 32 (2007) 3664–3671.
- [14] M. Krumpelt, T.A. Cruse, B.J. Ingram, J.L. Routbort, S.L. Wang, P.A. Salvador, G. Chen, J. Electrochem. Soc. 157 (2010) B228–B233.
- [15] A.A. Kulikovskiy, J. Electrochem. Soc. 158 (2011) B253–B258.
- [16] J.A. Schuler, C. Gehrig, Z. Wuillemin, A.J. Schuler, J. Wochele, C. Ludwig, A. Hessler-Wyser, J. Van Herle, J. Power Sources 196 (2011) 7225–7231.
- [17] S.P. Simner, M.D. Anderson, G.G. Xia, Z. Yang, L.R. Pederson, J.W. Stevenson, J. Electrochem. Soc. 152 (2005) A740–A745.
- [18] B.B. Ebbinghaus, Combust. Flame 93 (1993) 119–137.
- [19] C. Gindorf, L. Singheiser, K. Hilpert, J. Phys. Chem. Solids 66 (2005) 384–387.
- [20] K. Hilpert, D. Das, M. Miller, D.H. Peck, R. Weiss, J. Electrochem. Soc. 143 (1996) 3642–3647.
- [21] E.J. Opila, D.L. Myers, N.S. Jacobson, I.M.B. Nielsen, D.F. Johnson, J.K. Olminsky, M.D. Allendorf, J. Phys. Chem. A 111 (2007) 1971–1980.
- [22] R. Sachitanand, M. Sattari, J.E. Svensson, J. Froitzheim, Int. J. Hydrogen Energy 38 (2013) 15328–15334.
- [23] D. Chatterjee, S. Biswas, Int. J. Hydrogen Energy 36 (2011) 4530–4539.
- [24] P.E. Gannon, V.I. Gorokhovskiy, M.C. Deibert, R.J. Smith, A. Kayani, P.T. White, S. Sofie, Z. Yang, D. McCready, S. Visco, C. Jacobson, H. Kurokawa, Int. J. Hydrogen Energy 32 (2007) 3672–3681.
- [25] M. Stanislawski, J. Froitzheim, L. Niewolak, W.J. Quadackers, K. Hilpert, T. Markus, L. Singheiser, J. Power Sources 164 (2007) 578–589.
- [26] R. Trebbels, T. Markus, L. Singheiser, J. Electrochem. Soc. 157 (2010) B490–B495.
- [27] J. Froitzheim, S. Canovic, M. Nikumaa, R. Sachitanand, L.G. Johansson, J.E. Svensson, J. Power Sources 220 (2012) 217–227.
- [28] J. Froitzheim, H. Ravash, E. Larsson, L.G. Johansson, J.E. Svensson, J. Electrochem. Soc. 157 (2010) B1295–B1300.
- [29] J.G. Grolig, H. Abdesselam, M. Gas, H.F. Windisch, J. Froitzheim, J.E. Svensson, Solid Oxide Fuel Cells 13 (Sofc-Xiii) 57 (2013) 2339–2347.
- [30] J.G. Grolig, J. Froitzheim, J.E. Svensson, J. Power Sources 248 (2014) 1007–1013.
- [31] J. Froitzheim, J.E. Svensson, Ecs Trans. 35 (2011) 2503–2508.
- [32] M.R. Ardigo, I. Popa, S. Chevalier, C. Desgranges, R. Bousquet, Int. J. Hydrogen Energy 37 (2012) 8177–8184.
- [33] L.L. Zheng, J.J. Li, M.S. Li, Y.C. Zhou, Int. J. Hydrogen Energy 37 (2012) 1084–1088.
- [34] J.H. Zhu, S.J. Geng, D.A. Ballard, Int. J. Hydrogen Energy 32 (2007) 3682–3688.
- [35] D.J.L. Brett, A. Atkinson, N.P. Brandon, S.J. Skinner, Chem. Soc. Rev. 37 (2008) 1568–1578.
- [36] J. Hayd, L. Dieterle, U. Guntow, D. Gerthsen, E. Ivers-Tiffée, J. Power Sources 196 (2011) 7263–7270.
- [37] A. Jaiswal, E.D. Wachsman, J. Electrochem. Soc. 152 (2005) A787–A790.
- [38] K.T. Lee, H.S. Yoon, E.D. Wachsman, J. Mater. Res. 27 (2012) 2063–2078.
- [39] Z.P. Shao, S.M. Haile, Nature 431 (2004) 170–173.
- [40] S.F. Wang, Y.F. Hsu, H.C. Lu, C.C. Huang, C.T. Yeh, Int. J. Hydrogen Energy 37 (2012) 12548–12556.
- [41] S.F. Wang, C.T. Yeh, Y.R. Wang, Y.F. Hsu, J. Power Sources 201 (2012) 18–25.
- [42] H. Asteman, J.E. Svensson, M. Norell, L.G. Johansson, Oxid. Met. 54 (2000) 11–26.
- [43] M. Casteel, D. Lewis, P. Willson, M. Alinger, Int. J. Hydrogen Energy 37 (2012) 6818–6829.
- [44] S.J. Geng, J.H. Zhu, M.P. Brady, H.U. Anderson, X.D. Zhou, Z.G. Yang, J. Power Sources 172 (2007) 775–781.
- [45] L. Ge, A. Verma, R. Goettler, D. Lovett, R.K.S. Raman, P. Singh, Metall. Mater. Trans. A 44A (2013) 193–206.
- [46] P. Huczowski, S. Ertl, J. Piron-Abellan, N. Christiansen, T. Hofler, V. Shemet, L. Singheiser, W.J. Quadackers, Mater. High Temp. 22 (2005) 253–262.
- [47] I.H. Jung, Solid State Ionics 177 (2006) 765–777.
- [48] S. Canovic, J. Froitzheim, R. Sachitanand, M. Nikumaa, M. Halvarsson, L.G. Johansson, J.E. Svensson, Surf. Coatings Technol. 215 (2013) 62–74.
- [49] C.S. Tedmon, J. Electrochem. Soc. 113 (1966) 766.
- [50] T. Brylewski, J. Dabek, K. Przybylski, J. Therm. Anal. Calorim. 77 (2004) 207–216.
- [51] H. Hindam, D.P. Whittle, Oxid. Met. 18 (1982) 245–284.
- [52] E.A. Gulbransen, K.F. Andrew, J. Electrochem. Soc. 104 (1957) 334–338.
- [53] K.Q. Huang, P.Y. Hou, J.B. Goodenough, Solid State Ionics 129 (2000) 237–250.
- [54] A.W.B. Skilbred, R. Haugsrud, J. Power Sources 206 (2012) 70–76.
- [55] A.M. Huntz, A. Reckmann, C. Haut, C. Severac, M. Herbst, F.C.T. Resende, A.C.S. Sabioni, Mat. Sci. Eng. a-Struct. 447 (2007) 266–276.
- [56] A.C.S. Sabioni, A.M. Huntz, M.F. Salgado, A. Pardini, E.H. Rossi, R.M. Paniago, V. Ji, Mater. High Temp. 27 (2010) 89–96.
- [57] W.C. Hagel, A.U. Seybolt, J. Electrochem. Soc. 108 (1961) 1146–1152.
- [58] I. Panas, J.E. Svensson, H. Asteman, T.J.R. Johnson, L.G. Johansson, Chem. Phys. Lett. 383 (2004) 549–554.